Magnetic behavioural change of silane exposed graphene nanoflakes

Magnetic behavioural change of silane exposed graphene nanoflakes

Sekhar C. Ray' , D. K. Mishra, A. M. Strydom, and P. Papakonstantinou

Citation: J. Appl. Phys. **118**, 115302 (2015); doi: 10.1063/1.4930932
View online: http://dx.doi.org/10.1063/1.4930932
View Table of Contents: http://aip.scitation.org/toc/jap/118/11
Published by the American Institute of Physics

Magnetic behavioural change of silane exposed graphene nanoflakes

Sekhar C. Ray,[1,a)] D. K. Mishra,[1,2] A. M. Strydom,[3] and P. Papakonstantinou[4]
[1]*Department of Physics, College of Science, Engineering and Technology, University of South Africa, Private Bag X6, Florida, 1710, Science Campus, Christiaan de Wet and Pioneer Avenue, Florida Park, Johannesburg 1710, South Africa*
[2]*Department of Physics, Institute of Technical Research and Education, Siksha 'O' Anusandhan University, Khandagiri Square, Bhubaneswar 751030, Odisha, India*
[3]*Highly Correlated Matter Research Group, Physics Department, University of Johannesburg, PO Box 524, Auckland Park 2006, South Africa*
[4]*Nanotechnology and Integrated Bioengineering Center (NIBEC), School of Engineering, University of Ulster, Jordanstown Campus, Newtownabbey BT37 0QB, United Kingdom*

(Received 24 May 2015; accepted 1 September 2015; published online 15 September 2015)

The electronic structures and magnetic properties of graphene nanoflakes (GNFs) exposed to an organo-silane precursor [tetra-methyl-silane, $Si(CH_3)_4$] were studied using atomic force microscopy, electron field emission (EFE), x-ray photoelectron spectroscopy (XPS), and magnetization. The result of XPS indicates that silyl radical based strong covalent bonds were formed in GNFs, which induced local structural relaxations and enhanced sp^3 hybridization. The EFE measurements show an increase in the turn-on electric field from 9.8 V/μm for pure GNFs to 26.3 V/μm for GNFs:Si having highest Si/(Si + C) ratio ($\cong$0.35) that also suggests an enhancement of the non-metallic sp^3 bonding in the GNFs matrix. Magnetic studies show that the saturation magnetization (Ms) is decreased from 172.53×10^{-6} emu/g for pure GNFs to 13.00×10^{-6} emu/g for GNFs:Si with the highest Si/(Si + C) ratio 0.35, but on the other side, the coercivity (Hc) increases from 66 to 149 Oe due to conversion of $sp^2 \rightarrow sp^3$-hybridization along with the formation of SiC and Si-O bonding in GNFs. The decrease in saturation magnetization and increase in coercivity (Hc) in GNFs on Si-functionalization are another routes to tailor the magnetic properties of graphene materials for magnetic device applications. [http://dx.doi.org/10.1063/1.4930932]

I. INTRODUCTION

Graphene[1] has attracted tremendous attention in diverse areas due to its extraordinary properties, such as high aspect ratio, large surface area, and unique electronic structures.[2–5] Graphene is a zero-band gap semiconductor and exhibits semi-metallic behaviour. The lack of a band gap renders the feasibility of graphene based semiconductor devices, such as field-effect transistors (FETs)[1] and spintronics application.[2] A large number of efforts have been adopted to tailor the electronic properties of graphene. Especially, the doping and/or functionalization with hetero-atoms are a very efficient way to tailor the properties of graphene.[6–8] Silicon atoms are frequently introduced into graphene as heteroatoms can improve and tune the properties of graphene.[9] It was observed by theoretical studies that the substitutionally doped Si atoms in CNTs and/or graphene were found to relax outwards and form sp^3 bonding.[10–12] Besides the single Si-impurity in monolayer graphene, Si doped bilayer/multi-layer graphene or graphene nano-ribbons/nano-flakes has been investigated, which shows that there is a covalent bonding of Si-atoms between different layers.[12,13] However, there are few experimental studies reported on Si-doped graphene and/or graphene nano-ribbons/nano-flakes, therefore it is important to give new insights into the electronic structure, chemical bonding, and their possible applications. Graphene nano flakes (GNFs), the derived graphene materials are quasi-two-dimensional networks of vertically aligned graphene sheets and have morphologies similar to those of nano carbon materials, such as carbon nanoflakes and nanosheets. The Si atoms chemisorbed on the surfaces of GNFs or CNTs provide dangling bonds, which may mediate the formation of other type of materials. The formation of sp^3 bonding in GNFs:Si can be expected to enhance their mechanical stability. On Si-doping, the band gap leads to an increase in effective mass and decrease the mobility because of defect scattering. Silicon doping in graphene structure has less destructive effect on graphene mobility due to resemblance of Si and C atoms. Silicon is a highly reactive centre that creates opportunities for silylated GNFs (GNFs:Si) to be used as novel nano-devices, such as chemical sensors and toxic gas scrubbers[14] and other possible electronic and storage devices. Very recently, Moulder *et al*. observed that the doping of Si-atoms into the network of graphene sheets increases the electro-catalytic activity for oxygen reduction reaction (ORR).[15]

In this report, we have investigated the interplay between silicon atoms in catalyst free graphene nano-flakes (GNFs) and we studied their electronic, electrical, and magnetic properties for the use of different electronic and magnetic storage devices.

II. EXPERIMENTAL DETAILS

GNFs with a thickness of ~1250 nm were synthesized directly on the Si substrate without catalyst by the

[a)]Author to whom correspondence should be addressed. Electronic mail: raysc@unisa.ac.za

microwave-plasma enhanced chemical vapor deposition (PECVD) process and were subsequently subjected to RF-plasma glow discharge with 35/5 and 0/40 Ar to tetramethylsilane [TMS, $Si(CH_3)_4$] gas ratios, respectively, at room temperature for 5 min.[16,17] These Si-treated GNFs are denoted as GNFs:Si. The core-level C *1s* XPS spectra were measured using the AXIS SUPRA x-ray photoelectron spectroscopy (XPS) equipment at UNISA. Electron field emission (EFE) characteristics were performed using a Keithley power supply (Keithley: model 237). The cathode voltage was applied by an analog programmable 1.0 kV power supply under computer control high resistance meter and the leakage current is less than 10^{-9} A in our system. The measured emission current was logged at each voltage. The measurements were carried out at room temperature under a low 10^{-6} Torr ambient pressure. The movement of the anode tip (1 mm diameter) was measured digitally, and the gap between emitter and collector was confirmed by optical microscope. During the measurements, the anode and cathode distance in the field emission system was fixed at 200 μm, which is the thickness of the microglass spacer used to isolate the cathode from the anode. The magnetization (M) as function of applied field H was measured using a superconducting quantum interference device (SQUID) magnetometer (Quantum Design, San Diego). The surface morphology was studied by Atomic force microscopy (AFM) images (Nanoscope III, Veeco), which were captured in tapping mode using SiN tip with dimension 5–10 nm.

III. RESULTS AND DISCUSSION

Figures 1(a)–1(c) present the AFM images of pure GNFs and GNFs:Si, whereas Figures 1(d)–1(f) show EFE, current density (J) as a function of the applied electric field (E_A). Pure GNFs (1a) contain petal-like graphitic nano-flakes with sharp edges, which are randomly interlaced to form a nest-like porous structure with a large surface area;[16,17] whereas Si-functionalized GNFs as shown in Figures 1(b) and 1(c) show round nano-flakes in the form of rod- or tube like GNFs:Si. These transformations of GNFs:Si shapes/sizes indicate the transformation of GNFs:Si surficial structural behaviours. The EFE figure shows the existence of a threshold electric field, at which J increases from zero significantly. In general, the threshold electric field increases with the increase in the Si content that shows J increases roughly exponentially beyond the threshold field. To further demonstrate the existence of a threshold electric field or turn-on electric field (E_{TOE}), Fowler-Nordheim (F-N) plots are shown in insets (d)–(f) of Figure 1. The E_{TOE} values were obtained with linear curve fitting in the lower electric field region (not shown in this figure) and were found to increase from 9.8 V/μm for pure GNFs to 26.3 V/μm for GNFs:Si with the highest Si/(Si + C) ratio 0.35 (see Table I).

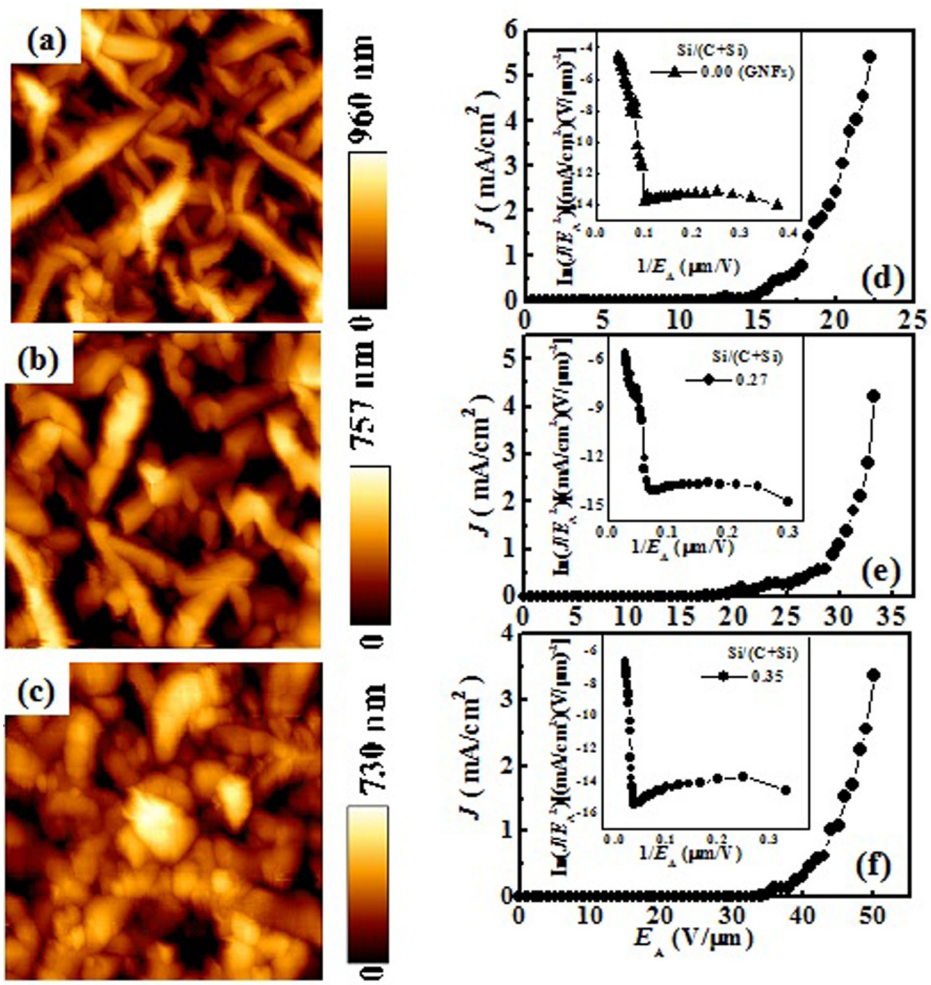

FIG. 1. Atomic Force Microscopy (AFM) images and Electron Field Emission (EFE) of (a) and (d) GNFs, (b) and (e) GNFs:Si (Si/Si + C = 0.27), and (c) and (f) GNFs:Si (Si/Si + C = 0.35).

TABLE I. Compositional and quantitative analysis of GNFs and GNFs:Si along with turn on electric field (E_{TOE}) obtained from F-N plots.

Sample	Ar/TMS (sccm)	C (at. %)	O (at. %)	Si (at. %)	Si/(Si + C) ratio	E_{TOE} (V/μm)
GNFs	—	97.55	2.45	0.00	0.00	9.8
GNFs:Si	35/5	54.41	25.09	20.50	0.27	15.9
GNFs:Si	0/40	39.34	39.15	21.51	0.35	26.3

The turn-on electric field is defined at an emission current density of 10^{-6} A/cm^2, i.e., the GNFs at higher Si-content need higher electric field to obtain the same current. This reduction in field emission current (or increase of turn on electric field) on Si-functionalization not only is attributed to the change in physical properties but also depends on the change in chemical properties that occur during the process of Si-functionalization. In terms of physical changes, it is observed from the AFM images as discussed above that the interlaced nest-like porous structure with a large surface area of pure GNFs reduced to round nano-flakes in the form of rod- or tube like GNFs:Si on Si-functionalization as shown in Figs. 1(a) and 1(c), respectively. However, the optimal surface morphology is not the only reason for the change in field emission characteristics, but the chemically Si-functionalization also have to be taken into account for the change of field emission characteristics. It was well known that the slope of FN plot is associated with the emission barrier expressed as $J = A(\beta E_A)^2 \exp(-B\phi^{3/2}/\beta E_A)$, in which A and B are constants, E_A is the applied electric field, β is the field enhancement factor, and ϕ is the emission barrier of the film. The fact that the slope of GNFs of highest Si/(Si + C) ratio 0.35 is obviously higher (see Fig. 1(f) inset) than that of pure GNFs (see Fig. 1(d) inset) suggests that the effective emission barrier is significantly increased due to silicon dilution and/or increase in $\phi^{3/2}/\beta$ factor. It can be deduced that the effective emission barrier of GNFs of highest Si/(Si + C) ratio 0.35 increased compared with that of pure FGNFs. On Si-functionalization, the formation of more sp^3-hybridized bonds in GNFs:Si is because Si prefers sp^3 rather than sp^2 bonding, unlike C (which prefers sp^2 bonding). The strong preference for sp^3 bonding was argued to be related to an outward relaxation of the Si atom.[10,11] Therefore, reduction of the EFE current in GNFs:Si is due to the decrease in the number of sp^2 hybridized bonds in the network of GNFs:Si because sp^2-hybridized bonds in GNFs are responsible for the metallic EFE current[18] in carbon structure materials. However, the optimal surface morphology is not the only reason for the change in field emission characteristics, but the chemical functionalization sites also have to be taken into account for the change of field emission. Hence, we measured the XPS of GNFs and Si-functionalized GNFs and discussed on this context in the following paragraph.

The chemical states of carbon atoms in GNFs films can be revealed by the XPS spectra of C1*s* core level. The XPS quantitative results indicate that the Si/(C + Si) ratios of GNFs:Si films are ≈0.27 and ≈0.35, respectively, when GNFs:Si is deposited at Ar/TMS ratios ≈5/35 and ≈0/40, respectively. The compositional and quantitative analysis of GNFs and GNFs:Si obtained from XPS analysis is tabulated in Table I. In general, the peak observed at ∼284.6 eV for GNFs can be assigned as the C-C bond (carbon sp^2-hybridization), which is shifted to the higher energy at ∼285.4 eV and became broaden for GNFs:Si having Si/(Si + C) of 0.35, as clearly shown in Figure 2(a). This peak shift indicates the change of structural and electronic behaviours. Figures 2(b)–2(d) show the decomposed C 1*s* XPS into Gaussian peaks of GNFs and GNFs:Si thin films. Figure 2(b) shows the decomposed GNFs spectrum into two peaks mainly at ∼284.2 eV and 286.1 eV which are assigned as C=C sp^2 and C-O bonds, respectively. The GNFs:Si spectra are decomposed into three peaks as shown in Figures 2(c) and 2(d). Pedio *et al.*[19] studied the dependence of the formation of C60 on silicon surfaces on the annealing temperature using C 1*s* XPS measurements and found that the C-C bond and C-Si bond features are located at 284.2 and 282.6 eV, respectively. We have observed a peak at ∼283.3 eV, which is in between the peaks 284.2 and 282.6 eV (films having Si/(Si + C) = 0.35) as shown in Figure 2(d) and is assigned as C-Si peak.[19,20] The peak observed at ∼283.9 eV and 284.5 eV in Figures 2(c) and 2(d), respectively, is assigned as C=C sp^2, whereas the peak 285.0 eV and 285.6 eV in Figures 2(c) and 2(d), respectively, is defined as "defect peaks"[16] or Si-C-O bonding peaks.[21] The peak observed in Figure 2(c) at 286.8 eV is the C-O bonds.[16] Figure 3 shows the Si 2p and 2s XPS spectra, where the main peaks are at∼100 eV and at ∼150 eV, respectively. However, these peaks are observed in

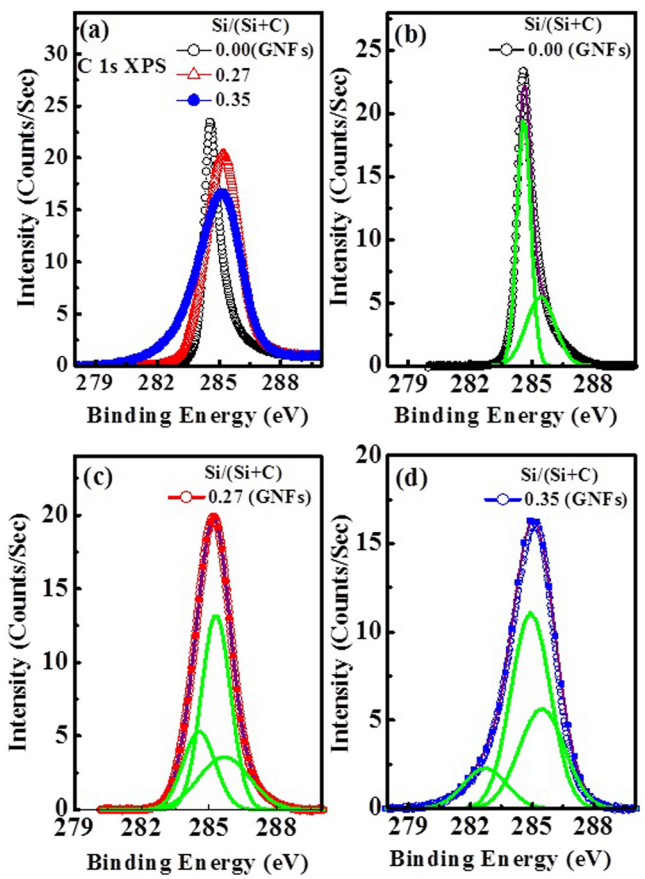

FIG. 2. C 1*s* x-ray photoemission spectroscopy (XPS) of (a) GNFs and GNFS:Si, (b) decomposed into two Gaussian peaks of GNFs, (c) decomposed into three Gaussian peaks of GNFs:Si (Si/Si + C = 0.27), and (d) decomposed into three Gaussian peaks of GNFs:Si GNFs:Si (Si/Si + C = 0.35).

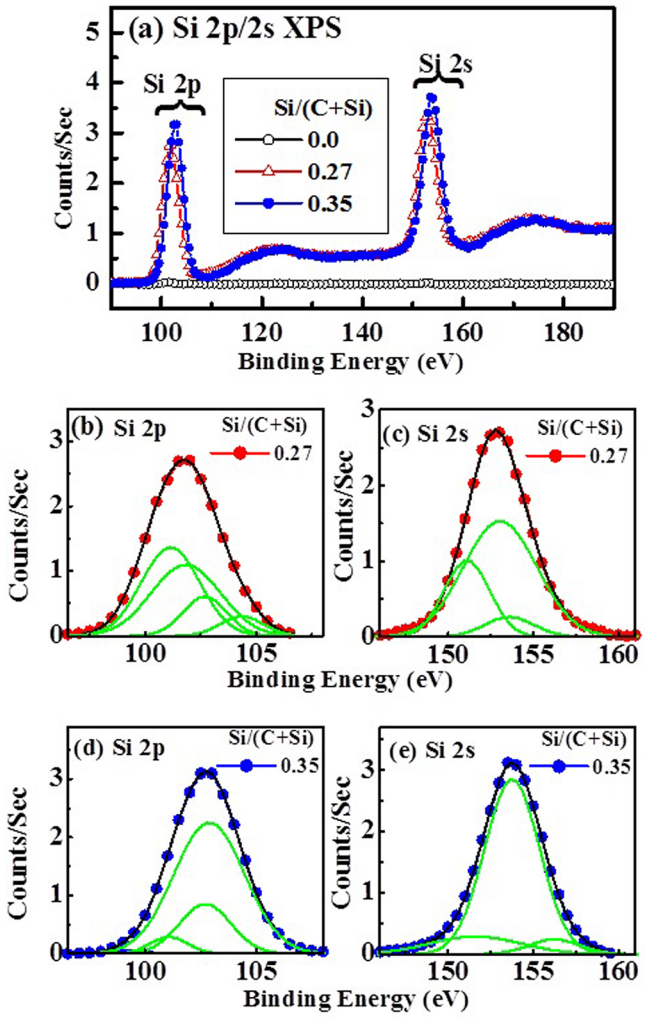

FIG. 3. Si 2*p*-2*s* x-ray photoemission spectroscopy (XPS) of (a) GNFs and GNFS:Si, (b) and (c) Si 2*p* and Si 2*s* decomposed into four and three Gaussian peaks, respectively, of GNFs:Si (Si/Si + C = 0.27). (d) and (e) Both Si 2*p* and Si 2*s* decomposed into three Gaussian peaks, respectively, of GNFs:Si (Si/Si + C = 0.35).

both GNFs:Si films that are decomposed into four (Si 2p) and three (Si 2s) Gaussian peaks and are shown in Figures 3(b) and 3(d) and 3(c) and 3(e), respectively. In case of Si 2p, the different decomposed peaks observed between ~101.00 eV and ~101.8 eV are assigned as Si-C/Si-C-O, whereas peaks observed between 102.4 eV and 104.3 eV are assigned as Si-O.[15,19,20] In case of Si 2s XPS, the peaks observed within the range ~151.1–153.0 eV are Si-Si peaks, whereas other peaks above 153.0 eV are assigned as Si-O.[22] It is very clear from these results that the changes of microstructural and bonding properties are of significance when Si is functionalized with GNFs that effect the change in electron field emission. It is also observed from the XPS decomposed peak intensity that on exposure to organo-silane (or Si-functionalization), the structures are changed from sp^2-rich to sp^3-rich ordered GNFs. From these results, it is very clear that the structural change occurs on Si-functionalized GNFs.

The magnetic properties of the GNFs and GNFs:Si are described through room-temperature (~300 K) and below room temperature (~40 K) field-dependent magnetization (M ~ H hysteresis loop) curves and these are shown in

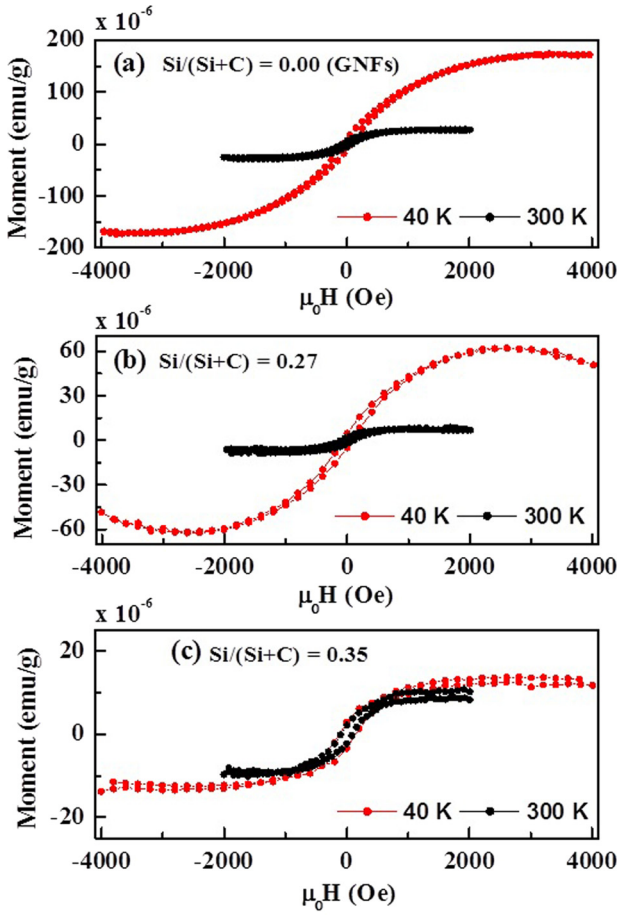

FIG. 4. The magnetic field-dependent magnetization M-H hysteresis loop curves at room temperature (~300 K) and below room temperature (40 K) of (a) GNFs, (b) GNFs:Si (Si/Si + C = 0.27), and (c) GNFs:Si (Si/Si + C = 0.35).

Figs. 4(a)–4(c). The magnetic results of GNFs:Si indicate primarily a weak paramagnetic behaviour at small field (≤100 Oe), but the field response at higher fields reveals non-monotonic, i.e., M is non-linear with H. A slender and saturation-prone (above ~2000 Oe) hysteresis loop is observed for all the GNFs/GNFs:Si, which suggests ferromagnetic behaviour. All the GNFs have different saturation magnetization (M_S), indicating that the Si-nano-crystals on the GNFs:Si change the structural behaviours. The saturation magnetization values of GNFs, $M_S \approx 173 \times 10^{-6}$ emu/g when measured at 40 K. This M_S value reduced to $\approx 62 \times 10^{-6}$ emu/g and $\approx 13 \times 10^{-6}$ emu/g, respectively, for GNFs:Si films, when the Si/(Si + C) ratios are 0.27 and 0.35, respectively. The saturation magnetization (M_S), coercivity (H_C), and remanence (M_R) of GNFs and GNFs:Si are tabulated in Table II. It shows that the M_S values are reduced with increasing coercivity as the Si-content is increased, implying the loss of magnetization with silicon content. With increase in Si-content, non-defect Si-C tetrahedral bonding along with SiO is formed that makes sp^3-rich structured GNFs materials that are responsible for reducing the magnetisation of GNFs. The observation of decrease in magnetic behaviour suggests that Si incorporation into GNFs forms a strong interaction in the form of Si-C, which is tetrahedral bonded. The formation of these bonds reduces the sp^2 hybridization present in the bare-GNFs and

TABLE II. Saturation magnetization (M_S), coercivity (H_C), and remanence (M_R) of GNFs and GNFs:Si.

Sample	Si/(Si + C) ratio	M_s ($\times 10^{-6}$ emu/g)		H_c (Oe)		M_R ($\times 10^{-6}$ emu/g)	
		40 K	300 K	40 K	300 K	40 K	300 K
GNFs	0.00	172.53	27.19	66.00	81.27	9.38	5.83
GNFs:Si	0.27	62.05	6.92	90.00	108.00	4.62	2.25
GNFs:Si	0.35	13.00	12.00	149.00	101.00	2.85	2.20

increases the sp^3 hybridisation concentration due to tetrahedral bonded Si with C. However, during and/or after synthesis of pure GNFs, the oxygen contamination occurs with Si upon air exposure and forms Si-O bonds. As a consequence, it reacts with carbon containing GNFs and forms clusters like Si-O-C, known as a defect structure that is responsible for the reducing of ferromagnetic behaviours. It is very interesting that the GNFs:Si having Si/(Si + C) ratio 0.35, reduces the saturation magnetization significantly, compared to pure GNFs when measured at 40 K. At 300 K, full magnetization is achieved, regardless of the Si content, in a field of ~1000 Oe. Much lower at 40 K on the other hand, we notice the Si-free GNFs (Fig. 4(a)) to be the least susceptible towards saturation, and with an increasingly facile saturation as Si is introduced in GNFs (Figs. 4(b) and 4(c) at 40 K). Whereas the magnetic moment achieved at high field (2000 Oe) and high temperature (300 K) is almost unchanged for all GNFs, the low temperature results further express a nearly 20-fold decrease in the high field moment as the Si content is increased from zero to Si/(Si + C) = 0.35. The high Si-content GNFs evidently have a near temperature-independent magnetic susceptibility between 300 K and 40 K compared to strong T-dependence that is found in the Si-free GNFs. We ascribe this to be the parasitic effect that Si has in this system on the p-electrons, namely, the increasingly effective $sp^2 \rightarrow sp^3$ hybridization which consumes p-electrons. It is also further observed that the saturation magnetization does not vary significantly at 300 K and 40 K temperature for the GNFs:Si [Si/(Si + C) = 0.35] that implies the structural ordering between Si and C is very much minimum as the concentration of Si/(Si + C) increases. It is reported in literature[23] that the incorporation of Si in graphene transforms the semi-metallic magnetic graphene to semiconducting magnetic graphene which has a large area of application FETs and in spintronics devices. In typical spintronics application, the materials should have semiconducting as well as magnetic behaviour. In this present study, Si is a good candidate to provide both semiconducting as well as magnetic properties in GNFs. We have demonstrated that controlled Si-functionalization of GNFs is a useful tool to manipulate the magnetic properties. At the same time, Si-functionalization enables tuning of the semiconducting properties and thus should be opening a new path for applications in spintronic devices.

IV. CONCLUSION

In conclusion, the structure of GNFs changes from sp^2 to sp^3 hybridized comparatively hard GNFs materials along with formation of Si-Si, Si-C, and Si-O/Si-O-C bonding and their magnetic behaviours are changed with addition of silicon in the GNFs matrix structure. Our magnetic studies have shown that Si-functionalization is another route to tailor the magnetic properties of GNFs materials and typically can be considered as an alternative route to tailor the magnetic properties of graphene for magnetic device applications.

ACKNOWLEDGMENTS

The author S.C.R. acknowledges to National Research Foundation (NRF), South Africa for financial support. AMS acknowledges support from the FRC and URC of UJ, and from the SA-NRF (93549).

[1]K. S. Novoselov, A. K. Geim, S. V. Morozov, D. Jiang, Y. Zhang, S. V. Dubonos, I. V. Grigorieva, and A. A. Firsov, Science **306**, 666–669 (2004).
[2]P. San-Jose, E. Prada, E. McCann, and H. Schomerus, Phys. Rev. Lett. **102**, 247204 (2009).
[3]F. Schedin, A. K. Geim, S. V. Moeozov, E. W. Hill, P. Blake, M. I. Katsnelson, and K. S. Novoselov, Nature Mater. **6**, 652–655 (2007).
[4]I. I. Barbolina, K. S. Novoselov, S. V. Morozov, S. V. Dubonos, M. Missous, A. O. Volkov, D. A. Christian, I. V. Grigorieva, and A. K. Geim, Appl. Phys. Lett. **88**, 013901 (2006).
[5]D. S. L. Abergel, V. Apalkov, J. Berashevich, K. Ziegler, and T. Chakraborty, Adv. Phys. **59**, 261–482 (2010).
[6]J. Dai, J. Yuan, and P. Giannozzi, Appl. Phys. Lett. **95**, 232105 (2009).
[7]Y. Yong, B. Song, K. Liu, and P. He, J. Appl. Phys. **111**, 083713 (2012).
[8]X.-L. Wei, H. Fang, R.-Z. Wang, Y.-P. Chen, and J.-X. Zhong, Appl. Phys. Lett. **99**, 012107 (2011).
[9]Y. Chen, B. Gao, J. X. Zhao, Q. H. Cai, and H. G. Fu, J. Mol. Model. **18**, 2043–2054 (2012).
[10]R. J. Baierle, S. B. Fagan, R. Mota, A. J. R. da Silva, and A. Fazzio, Phys. Rev. B **64**, 085413 (2001).
[11]S. B. Fagan, R. Mota, R. J. Baierle, A. J. R. da Silva, and A. Fazzio, Diamond Relat. Mater. **12**, 861 (2003).
[12]C. W. Pao, S. C. Ray, H. M. Tsai, Y. S. Chen, H.-C. Chen, I.-N. Lin, W. F. Pong, J. W. Chiou, M.-H. Tsai, N. G. Shang, P. Papakonstantinou, and J.-H. Guo, J. Phys. Chem. C **114**, 8161–8166 (2010).
[13]H. J. Xiang, B. Huang, Z. Y. Li, S.-H. Wei, J. L. Yang, and X. G. Gong, Phys. Rev. X **2**, 011003 (2012).
[14]G. Guo, F. Wang, H. Sun, and D. Zhang, Int. J. Quantum Chem. **108**, 203–209 (2008).
[15]J. F. Moulder, W. F. Stickle, P. E. Sobel, and K. D. Bomben, *Handbook of X-Ray Photoelectron Spectroscopy—A Reference Book of Standard Spectra for Identifications and Interpretation of XPS Data* (Perkin-Elmer Corporation, Eden Prairie, MN, 1992).
[16]N. G. Shang, P. Papakonstantinou, M. McMullan, M. Chu, A. Stamboulis, A. Potenza, S. S. Dhesi, and H. Marchetto, Adv. Funct. Mater. **18**, 3506 (2008).
[17]G. A. Abbas, P. Papakonstantinou, J. A. D. McLaughlin, T. D. M. Weijers-Dall, R. G. Elliman, and J. Filik, J. Appl. Phys. **98**, 103505 (2005).
[18]S. C. Ray, U. Palnitkar, C. W. Pao, H. M. Tsai, W. F. Pong, I.-N. Lin, P. Papakonstantinou, L. C. Chen, and K. H. Chen, J. Appl. Phys. **104**, 063710 (2008).
[19]M. Pedio, F. Borgatti, A. Giglia, N. Mahne, S. Nannarone, S. Giovannini, C. Cepek, E. Magnano, G. Bertoni, E. Spiller, M. Sancrotti, L. Giovanelli, L. Floreano, R. Gotter, and A. Morgante, Phys. Scr., T **115**, 695 (2005).
[20]G. Račiukaitis, M. Brikas, V. Kazlauskienė, and J. Miškinis, J. Phys.: Conf. Ser. **59**, 150–154 (2007).
[21]T. Maruyama and S. Naritsuka, "Nanotechnology and Nanomaterials: Carbon Nanotubes - Synthesis, Characterization, Applications," edited by Siva Yellampalli, Department of Material Science and Engineering, Meijo University, Japan, see www.intechopen.com.
[22]Y. J. Choi, S.-J. Won, H.-S. Jung, S. Park, D.-Y. Cho, C. S. Hwang, T. J. Park, and H. J. Kima, ECS Solid State Lett. **1**, N4–N6 (2012).
[23]M. S. S. Azadeh, A. Kokabi, M. Hosseini, and M. Fardmanesh, Micro Nano Lett. **6**, 582–585 (2011).